Journal of Nuclear Medicine, published on October 12, 2017 as doi:10.2967/jnumed.117.191221

Low level endogenous prostate-specific membrane antigen (PSMA) expression in non-prostatic tumor xenografts is sufficient for in vivo tumor targeting and imaging

Sridhar Nimmagadda[1,2], Mrudula Pullambhatla[1], Ying Chen[1], Princy Parsana, Ala Lisok[1], Samit Chatterjee[1], Ronnie Mease[1,2], Steven P. Rowe[1], Shawn Lupold[24], Kenneth J. Pienta[2,4], and Martin G. Pomper[1,2,4]

[1]Russell H. Morgan Department of Radiology and Radiological Science,

[2]Sidney Kimmel Comprehensive Cancer Center,

[3]Department of Computer Science

[4]The James Buchanan Brady Urological Institute & Department of Urology,

Johns Hopkins Medical Institutions, Baltimore, MD, 21287.

*Corresponding author: Sridhar Nimmagadda, Ph.D, Johns Hopkins Medical Institutions, 1550 Orleans Street, CRB II, #491, Baltimore, MD 21287, Phone: 410-502-6244, Fax: 410-614-3147, Email: snimmag1@jhmi.edu

Word Count: 5277

Financial support. We gratefully acknowledge grant support from NIH R01CA134675, U01 CA183031, R01 CA184228 (MGP) and Allegheny-Hopkins Network Cancer Research Fund (SN).

Key words: Prostate cancer, melanoma, lung cancer, molecular imaging, CCLE, TCGA

Running title: PSMA imaging in non-prostate cancers

ABSTRACT

Prostate-specific membrane antigen (PSMA) is highly expressed in prostate cancer and within the neovasculature of other solid tumors. The non-prostatic expression of PSMA has been reported exclusively within the neovasculature endothelial cells of non-prostate cancers, however, there are few reports on PSMA expression on epithelial cells. Herein we describe PSMA expression in non-prostatic epithelial cells and characterize the potential of PSMA-binding agents to non-invasively detect that expression. **Methods.** PSMA expression data was extracted from publicly available genomic databases. Genomic data was experimentally validated for PSMA expression, by quantitative **reverse transcription** polymerase chain reaction (RT-qPCR), flow cytometry and western blotting, in several non-prostatic cell lines and xenografts of melanoma and small cell lung cancer (SCLC) origin. Feasibility of PSMA detection in those tumor models was further established using PSMA-based nuclear and optical imaging agents and by biodistribution, blocking, and *ex vivo* molecular characterization studies. **Results**. We discovered that a small percentage of non-prostatic cancer cell lines and tumors express PSMA. Importantly, PSMA expression was sufficiently high to image established melanoma and SCLC xenografts using PSMA-based nuclear and optical imaging agents. **Conclusions**. These results indicate that PSMA expression in non-prostatic tumors may not be limited to the endothelium but may also include solid tumor tissue of non-prostate cancers including melanoma and SCLC. Our observations indicate broader applicability of PSMA targeted imaging and therapeutics.

INTRODUCTION

PSMA, also known as folate hydrolase (FOLH1) or glutamate carboxypeptidase II, is a type-2 integral membrane protein with zinc-dependent exopeptidase activity (*1,2*). PSMA expression in healthy human tissues is present within the secretory-acinar epithelium of the prostate, proximal tubules of the kidney, astrocytes and Schwann cells of the nervous system, salivary glands, ovaries and testes (*3*). In prostate cancer, elevated PSMA expression and alternative splicing produce high levels of PSMA protein on the surface of prostate cancer cells. Nearly 95% of prostate cancers are reported to have elevated PSMA expression (*4,5*). Over the past decade PSMA has gained considerable attention as an imaging and therapeutic target because of its elevated expression within malignant prostate tissues, its presentation on the cell surface, and its rapid cellular internalization kinetics (*6*).

PSMA expression on the endothelial cells of tumor-associated neovasculature has been described in non-prostate cancers but its expression on epithelial cells has not been well characterized (*7,8*). Our analysis of large-scale cancer cell line derived genomic data sets revealed the presence of PSMA in many non-prostate cancer cell lines, which was corroborated by transcript levels observed in human tumors. We then sought to experimentally validate those observations by in vitro and in vivo characterization of PSMA expression in multiple cancer cell lines and the corresponding tumor xenografts. We also evaluated the potential of existing PSMA targeted imaging agents to non-invasively assess PSMA expression in tumor xenografts derived from those cell lines. Our results in several tumor models of melanoma and SCLC origin demonstrate that PSMA expression in non-prostate epithelial cancer cells is sufficiently high enough to be detected using single photon emission computed tomography (SPECT) and near-

infrared (NIR) imaging methods. Our results support the view that PSMA-based imaging agents and therapeutics could have much broader applicability in non-prostate tumors.

MATERIALS AND METHODS

Analysis of CCLE and TCGA data

mRNA expression data, in log 2 counts, was downloaded from the Cancer Cell Line Encyclopedia database (CCLE) and converted to z-scores using all of the cell lines as a reference population. Upper quartile normalized RSEM count estimates of RNASeqV2 data were downloaded for 19 cancer types from The Cancer Genome Atlas (TCGA). FOLH1 gene counts were extracted for these cancer types and converted to $\log_2$ counts. Samples with missing values and NaNs were eliminated. Gene expression analysis was performed using the R statistical programming environment. The results presented here are based upon data generated by the TCGA Research Network.

Cell Culture

The human prostate cancer cell lines, PSMA+ PC3 PIP and PSMA- PC3 flu(*9*), human melanoma cell lines, SKMEL3 and MeWo, and human SCLC cell lines, DMS53 and H69 were cultured in RPMI1640 medium containing 10% fetal bovine serum and 1% penicillin-streptomycin. The human melanoma cell line SKMEL24 was grown in RPMI1640 medium containing 15% fetal bovine serum, 1 mM sodium pyruvate, 0.1 mM non-essential amino acids and 1.5 g/L sodium bicarbonate. Immortalized normal prostate epithelial RWPE-1 cells were cultured in keratinocyte serum free medium supplemented with 0.05 mg/mL of bovine pituitary extract and 5 ng/mL of epidermal growth factor. All cell lines grown to 80% confluence were used for *in vitro* and *in vivo* studies. PSMA expression on PSMA+ PC3-PIP cells was routinely screened by flow cytometry. SKMEL24, SKMEL3, MeWo and H69 cell lines were purchased

from ATCC (Manassas, VA), cultured for less than six months following resuscitation and were not authenticated. The DMS53 cell line was a gift from Dr. Rajani Ravi of Johns Hopkins and was authenticated in the Johns Hopkins genetic resources facility.

Flow Cytometry

Adherent cells were detached using enzyme-free cell dissociation buffer (Gibco) and suspension cells were harvested by centrifugation. The harvested cells were washed twice with flow cytometry buffer (1x phosphate buffered saline with 2 mM ethylenediaminetetraacetic acid and 0.5 % fetal bovine serum), and stained with anti-human PSMA antibody conjugated with phycoerythrin (Bioegend, catalog # 341503, clone LNI-17) according to the manufacturer's protocol. PSMA expression was analyzed on a FACSCalibur flow cytometer (Becton Dickinson). Data analysis was carried out using FlowJo software (Tree Star).

Tumor Models

Animal studies were performed according to the protocols approved by the Johns Hopkins University Animal Care and Use Committee. Four- to six-week-old male non-obese diabetic severe combined immunodeficiency (NOD/SCID) mice were purchased from the Johns Hopkins Immune-compromised Mouse Core for *in vivo* experiments. For tumor generation, 3 x 10^6 cells of SKMEL3 or MeWo were injected subcutaneously (s.c.) in the forward right and left flanks, respectively. SKMEL24 or DMS53 tumor-bearing mice were generated by s.c. injection of 5 x 10^6 cells in separate groups of mice. H69 tumor bearing mice were generated by tumor passage of a previously snap-frozen H69 tumor. PSMA+ PC3 PIP and PSMA- PC3 flu tumor-bearing mice were generated by s.c. injection of 1 x10^6 cells of each cell line in the forward right and left flanks, respectively. Mice were used in *in vivo* experiments when the tumors reached a size of at least 100-300 mm^3.

Radiosynthesis, SPECT-CT imaging, Ex vivo Biodistribution, RT-qPCR, Immunohistochemistry and Immunoblot

The radiosynthesis of a known PSMA imaging agent ^{125}I-DCIBzl was performed as described previously (*9*). Detailed radiosynthesis, SPECT imaging and biodistribution, RT-qPCR, immunohistochemistry and immunoblot methods are described in the supplementary methods section.

Fluorescence Imaging

PSMA binding IRDye® 800CW YC-27 (YC-27) was purchased from LI-COR Biosciences (Lincoln, NE). Detailed optical imaging methods are imaging methods are described in the supplementary methods section.

Statistics

Statistical analyses were performed on Prizm 6.0 software (La Jolla, CA). The Student's unpaired t test was performed to determine statistical significance. All tests were two-sided, and *P*-values of < 0.05 were considered statistically significant. Error bars in the figures represent ± standard error of the mean (SEM).

RESULTS

PSMA Expression in Human Cancer Cell Line Derived CCLE and Primary Tumor Terived TCGA Data Sets

We queried PSMA gene expression levels (as *FOLH1*) in the publicly available CCLE database that contains genomic data from 1,047 cell lines. Prostate cancer cell lines showed the highest PSMA gene expression levels followed by skin cancer cell lines (Fig. 1A). Nearly 5% of CCLE cell lines showed PSMA gene expression levels higher than the median value of

the prostate cancer cell lines with several cell lines exhibiting at the level of prostate cancer cell lines.

We then investigated PSMA transcript levels in human tumors in TCGA. Transcript expression data from 21 tumor types show high PSMA levels in prostate cancers followed by cancers of kidney, liver and urothelium (Fig. 1B and supplemental table 1). Nearly 97% of prostate cancers exhibit PSMA transcripts and 12% of all the non-prostatic tumors show PSMA transcripts similar to or above the 1st quartile of prostate tumor transcript levels. Of those, ~10% were contributed by kidney, liver, urothelium, squamous lung and melanoma tumors and the remaining 1.4% representing all other cancers. Further analysis of individual cancer types showed that 57% of kidney, 39% of liver, 26% of urothelium, 21% of low grade glioma, 11.8% lung squamous cell carcinoma, and 9% skin cancers demonstrate PSMA transcript levels in the abovementioned range. Overall, high PSMA transcript levels were observed to be a non-frequent event in non-prostatic cancers. These data indicate that PSMA is expressed in a variety of non-prostate cancer epithelial cell lines and perhaps in tumors albeit at lower frequency than those of prostate.

Validation of PSMA Expression in Non-prostatic Cancer Cell Lines and Xenografts

To validate the PSMA positivity noted in the non-prostatic cancer cell lines in CCLE, we selected several that were either high (SKMEL24, SKMEL3, DMS53) or low (Mewo, H69) in PSMA expression and performed RT-qPCR and flow cytometry for gene and cell surface expression, respectively. RT-qPCR results showed that SKMEL24, SKMEL3 and DMS53 cells were PSMA+, with highest PSMA expression levels in SKMEL24 and SKMEL3 followed by DMS53 (Figure 2A). MeWo and H69 were negative for PSMA. Notably, PSMA expression in melanoma (SKMEL24, SKMEL3) and lung cells (DMS53) was considerably lower than that of prostate cells reflecting the CCLE data. PSMA positivity in these cell lines was also confirmed

in flow cytometric analyses, where PSMA expression in non-prostatic cells is 2-3 orders of magnitude lower than that of LnCap control cells (Figs. 2B & C) that overexpress copious amounts of PSMA (*10*). We next sought to confirm that PSMA expression was maintained *in vivo*. In subcutaneous xenograft tumors, PSMA expression was detected in SKMEL24, SKMEL3, and DMS53 tumors by RT-qPCR (Fig. 2D) and western blot (Figs. 2E & F). Gene and protein expression analyses showed highest PSMA expression levels in SKMEL24 and DMS53 followed by SKMEL3. The observed PSMA levels were also several orders of magnitude lower than those observed with PSMA+ PC3-PIP tumors. Collectively, data from melanoma and SCLC cell lines demonstrate cell surface PSMA expression on epithelial cells of non-prostate cancers.

Imaging PSMA expression in Non-prostate cancer Xenografts by SPECT Imaging

We then investigated whether PSMA expression in non-prostatic tumors is sufficiently high for non-invasive detection by PSMA-binding imaging agents.

Validation in melanoma models. We inoculated SKMEL24 cells subcutaneously into male mice and allowed tumors to establish. SPECT imaging of those mice at 60 min post-injection of ^{125}I-DCIBzl, an established PSMA SPECT imaging agent, showed accumulation and retention of radioactivity in the SKMEL24 tumors. Imaging at 24 h post-injection of ^{125}I-DCIBzl also demonstrated retention of radioactivity in the tumors (Fig. 3A). Accumulation of radioactivity in the tumors could be blocked by co-injection of the non-radiolabeled compound, confirming PSMA-mediated uptake.

We then investigated whether graded levels of PSMA expression could be imaged with PSMA-targeted imaging agents. To test this, we selected the SKMEL3 cell line with moderate expression of PSMA and the MeWo cell line that does not express PSMA. SPECT imaging of

mice harboring tumors showed specific but low accumulation of radioactivity in SKMEL3 tumors and almost no radiotracer uptake in MeWo tumors (Fig. 3B). Liver and kidney could also be clearly visualized, in line with previous studies (*9*). Further corroborating the imaging, biodistribution studies demonstrated graded radiotracer uptake in the tumors in proportion to the level of expression of PSMA in each cell line, namely, SKMEL24 > SKMEL3 > MeWo. The %ID/g for SKMEL24, SKMEL3 and MeWo tumors was 14.3 ± 1.5, 9.3 ± 0.4, and 1.2 ± 0.1, respectively. In mice that received a blocking dose, the %ID/g for SKMEL24, SKMEL3 and MeWo tumors was 1.7 ± 0.1, 1.1 ± 0.1, and 0.9 ± 0.1, respectively, indicating PSMA-mediated binding in the SKMEL24 and SKMEL3 tumor models (Fig. 3C). For molecular pathologic validation, biodistribution data in melanoma xenografts was confirmed by PSMA immunohistochemical analysis , which demonstrated intense and moderate PSMA immunoreactivity in SKMEL24 and SKMEL3 tumors, respectively. MeWo tumors did not show PSMA immunoreactivity (Fig. 3D). We have not observed PSMA immunoreactivity in the vasculature of these xenografts.

As additional positive and negative controls, we performed biodistribution studies in PSMA+ PC3 PIP and PSMA- PC3 flu tumors. ^{125}I-DCIBzl uptake in the PSMA+ PC3 PIP tumors was 29.9 ± 3.9 and that in the PSMA- PC3 flu tumors was 1.8 ± 0.4, further supporting the validity of the imaging agent (Supplemental Figure 1).

Confirmation in SCLC models. We next sought to confirm our observations in melanoma in a different tumor type. We chose SCLC cell lines DMS53 that has high PSMA and H69 that is PSMA negative. SPECT imaging of NOD/SCID mice bearing DMS53 tumors showed specific accumulation of radioactivity in tumors by 60 min that persisted at 24 h (Figs. 4A and B). Reduced radioactivity uptake was observed in the DMS53 tumors in the blocking study, demonstrating PSMA-specific binding (Fig. 4A). No appreciable accumulation of radioactivity

was observed in PSMA negative H69 tumors. The %ID/g observed in the biodistribution studies was 5.8 ± 0.7 and 0.9 ± 0.0 for DMS53 and H69 tumors, respectively. In mice receiving a blocking dose, the %ID/g was 0.8 ± 0.1 and 0.7 ± 0.1 for DMS53 and H69 tumors, respectively, indicating PSMA-mediated uptake in the former (Fig. 4C). Confirming the imaging and biodistribution studies, immunohistochemical analysis demonstrated moderate PSMA immunoreactivity in DMS53 tumors. PSMA immunoreactivity in H69 tumors was undetectable (Fig. 4D).

Collectively, these imaging, biodistribution and blocking studies demonstrated that PSMA expression in some of the non-prostate tumors is sufficiently expressed in the epithelial cell to be visualized by existing imaging agents.

Validation of PSMA Expression in Skin and Lung Cancer Xenografts by NIR Optical Imaging

Optical imaging agents are being exploited to develop photodynamic therapy and several low molecular weight PSMA-binding NIR optical imaging agents have been reported (*11-13*). One such agent, YC-27, previously reported by us, provides high target-to-non-target imaging specificity 24 h after injection. To investigate the feasibility of using PSMA-targeted optical imaging agents for detecting and targeting tumors with lower levels of PSMA expression, such as melanoma, we performed NIR imaging on mice bearing subcutaneous PSMA-positive SKMEL24 and SKMEL3 tumors, and PSMA-negative MeWo tumors, 24 h post-injection of YC-27. Results demonstrated significant accumulation of fluorescent signal in the SKMEL24 tumors and little to none in the melanotic SKMEL3 tumors (due to quenching) and PSMA-negative MeWo tumors. Similarly, in SCLC xenograft models, high fluorescence intensity was observed in PSMA+ DMS53 tumors but not in PSMA-negative H69 tumors (Fig. 5A). These qualitative observations were further supported by quantification of fluorescence intensity of

dissected tumors that showed a significant increase in fluorescence intensity in PSMA+ tumors (Fig. 5B).

DISCUSSION

PSMA expression in the tumor neovasculature of non-prostatic tumors is known and utilized for imaging and therapeutic purposes, however, its expression in epithelial cells of non-prostatic cancer has not been well characterized. By harnessing large-scale genomic data, we showed that non-prostatic cancer cell lines in the CCLE database have high PSMA gene expression. These observations in cell lines were supported by analysis of patient tumor derived TCGA data. High PSMA transcript levels in non-prostatic cancers occurred at low frequency and observed levels were similar to 1st quartile transcript levels in prostate cancers. We selected a few PSMA-positive melanoma and SCLC cell lines from CCLE, confirmed PSMA expression in cultured cells and subcutaneous xenografts, and demonstrated the potential of PSMA-targeting nuclear and optical agents to detect that expression. These results establish non-prostatic tumor models with epithelial cell PSMA expression and demonstrate that PSMA expression was sufficiently high for tumor targeting and imaging.

High-throughput sequencing has made precision medicine a reality (*14*). Availability of RNA sequencing data from a large number of cancer cell lines has allowed us to profile PSMA gene expression in various cancer cell lines. While prostate cancer cell lines showed high gene expression levels as anticipated, skin cancer cell lines were second highest. Notably, PSMA gene expression, although less frequent, was observed in many non-prostatic cell lines at a level similar to that of the prostate cancer cell lines. Several studies showed that protein levels and function are poorly predicted by genomic and transcriptomic analysis of patient-derived tumors, suggesting that further confirmation of protein expression and function is warranted even in cell lines expressing abundant transcript (*15*). In the limited number of cell lines we

investigated, eight in total, there was a strong correlation of PSMA transcript level with protein expression suggesting that transcript analysis could be indicative of PSMA expression in the tumors. These observations provide opportunities to tailor transcript data acquired from patient biopsies with existing PSMA imaging and therapeutics.

PSMA targeted imaging and therapeutic agents are making significant strides in prostate cancer diagnosis and treatment (*16-21*). However, despite the availability of excellent imaging agents (*22*), and the expression of PSMA in most solid tumor neovasculature, PSMA-targeted imaging has largely been limited to prostate cancer (*7,8,23,24*). Clinical case reports demonstrating PSMA expression in other cancers are appearing (*25-27*), although larger prospective trials that would confirm the clinical utility of PSMA agents in non-prostatic cancers have yet to be reported. Validation of existing PSMA imaging and therapeutic agents in non-prostatic tumors has been hampered by the lack of suitable models. Our results provide PSMA positive non-prostatic xenograft models for further validation of those imaging agents.

Due to the elevated expression of PSMA in prostate cancer, it has been leveraged as a diagnostic, drug delivery and immunomodulatory target for this disease (*28-30*). Several PSMA-targeted imaging and radiotherapeutic agents are under investigation for use in prostate cancer (*30-33*). ^{177}Lu-labeled J591 anti-PSMA antibody and several low molecular weight agents are now in clinical trials for treating micro-metastases (*34*). PSMA expression levels in tested non-prostatic cell lines and tumors is nearly 30 fold less than that observed in LnCap cell line, the applicability of which need to be further investigated for radiotherapy applications. Previous studies using ^{111}In-J591 to target the tumor neovasculature specifically has shown promising results in kidney, bladder, lung, breast, colorectal, and pancreatic cancers, and melanoma (*35*). Although earlier immunohistochemical analysis studies reported a lack of PSMA expression on epithelial cells of non-prostate tumors, few recent studies report PSMA expression on the

epithelial cells of non-prostatic cancers and metastatic nodules (*26,36*). PSMA targeted optical imaging agents are also being investigated as theranostic photosensitizers to deliver photodynamic therapy to prostate tumor xenografts (*37*). Our observations using PSMA optical imaging agents and their specific accumulation in PSMA positive non-prostatic tumor xenografts suggest a role for such agents in other tumor types. Taken together, our data show that PSMA expression in non-prostatic tumors is sufficiently high to be detected by existing PSMA imaging agents.

Recently, a PSMA-targeted imaging agent was used to detect metastatic nodules in a patient with clear cell renal carcinoma, although validation of PSMA expression by immunohistochemical analysis was not reported (*38*). While PSMA targeted therapeutics are being investigated and have shown therapeutic efficacy in patients with prostate cancer (*33,35,39*), their benefit for other cancers is not established. Melanoma and SCLC tumor models described in this work will provide an opportunity to evaluate these agents in preclinical models of non-prostatic cancers. Beyond any potential diagnostic utility, new theranostic treatment paradigms using PSMA-targeted endoradiotherapy may prove to be of particular value in diseases difficult to treat such as metastatic melanoma and SCLC.

CONCLUSION

We have demonstrated that PSMA is endogenously expressed in non-prostatic cancer cell lines and that expression in melanoma and SCLC is sufficiently high to be visualized using existing PSMA imaging agents. Also, we showed that graded levels of PSMA expression in non-prostatic cancer xenografts can be imaged using both nuclear and optical imaging agents. Our data suggests that certain non-prostatic tumors may express PSMA directly on the cancer cells, in addition to that previously reported in neovasculature.

ACKNOWLEDGEMENTS. We gratefully acknowledge grant support from NIH R01CA134675, U01 CA183031, R01 CA184228 (MGP) and Allegheny-Hopkins Network Cancer Research Fund (SN). We thank Dr. Jon Chung for help with CCLE data.

REFERENCES

1. Davis MI, Bennett MJ, Thomas LM, Bjorkman PJ. Crystal structure of prostate-specific membrane antigen, a tumor marker and peptidase. *Proc Natl Acad Sci U S A.* 2005;102:5981-5986.

2. Pavlicek J, Ptacek J, Barinka C. Glutamate carboxypeptidase II: an overview of structural studies and their importance for structure-based drug design and deciphering the reaction mechanism of the enzyme. *Curr Med Chem.* 2012;19:1300-1309.

3. Barinka C, Rojas C, Slusher B, Pomper M. Glutamate carboxypeptidase II in diagnosis and treatment of neurologic disorders and prostate cancer. *Curr Med Chem.* 2012;19:856-870.

4. Sweat SD, Pacelli A, Murphy GP, Bostwick DG. Prostate-specific membrane antigen expression is greatest in prostate adenocarcinoma and lymph node metastases. *Urology.* 1998;52:637-640.

5. Bostwick DG, Pacelli A, Blute M, Roche P, Murphy GP. Prostate specific membrane antigen expression in prostatic intraepithelial neoplasia and adenocarcinoma: a study of 184 cases. *Cancer.* 1998;82:2256-2261.

6. Ghosh A, Heston WD. Tumor target prostate specific membrane antigen (PSMA) and its regulation in prostate cancer. *J Cell Biochem.* 2004;91:528-539.

7. Chang SS, O'Keefe DS, Bacich DJ, Reuter VE, Heston WD, Gaudin PB. Prostate-specific membrane antigen is produced in tumor-associated neovasculature. *Clin Cancer Res.* 1999;5:2674-2681.

8. Chang SS, Reuter VE, Heston WD, Bander NH, Grauer LS, Gaudin PB. Five different anti-prostate-specific membrane antigen (PSMA) antibodies confirm PSMA expression in tumor-associated neovasculature. *Cancer Res.* 1999;59:3192-3198.

9. Chen Y, Foss CA, Byun Y, et al. Radiohalogenated prostate-specific membrane antigen (PSMA)-based ureas as imaging agents for prostate cancer. *J Med Chem.* 2008;51:7933-7943.

10. Kiess AP, Minn I, Chen Y, et al. Auger radiopharmaceutical therapy targeting prostate-specific membrane antigen. *J Nucl Med.* 2015;56:1401-1407.

11. Chen Y, Dhara S, Banerjee SR, et al. A low molecular weight PSMA-based fluorescent imaging agent for cancer. *Biochem Biophys Res Commun.* 2009;390:624-629.

12. Kelderhouse LE, Chelvam V, Wayua C, et al. Development of tumor-targeted near infrared probes for fluorescence guided surgery. *Bioconjug Chem.* 2013;24:1075-1080.

13. Lutje S, Rijpkema M, Goldenberg DM, et al. Pretargeted dual-modality immuno-SPECT and near-infrared fluorescence imaging for image-guided surgery of prostate cancer. *Cancer Res.* 2014;74:6216-6223.

14. Le DT, Uram JN, Wang H, et al. PD-1 blockade in tumors with mismatch-repair deficiency. *N Engl J Med.* 2015;372:2509-2520.

15. Akbani R, Ng PK, Werner HM, et al. A pan-cancer proteomic perspective on The Cancer Genome Atlas. *Nat Commun.* 2014;5:3887.

16. Szabo Z, Mena E, Rowe SP, et al. Initial evaluation of [(18)F]DCFPyL for prostate-specific membrane antigen (PSMA)-targeted PET imaging of prostate cancer. *Mol Imaging Biol.* 2015;17:565-574.

17. Rowe SP, Gage KL, Faraj SF, et al. (1)(8)F-DCFBC PET/CT for PSMA-based detection and characterization of primary prostate cancer. *J Nucl Med.* 2015;56:1003-1010.

18. Rowe SP, Macura KJ, Ciarallo A, et al. Comparison of prostate-specific membrane antigen-based 18F-DCFBC PET/CT to conventional imaging modalities for detection of hormone-naive and castration-resistant metastatic prostate cancer. *J Nucl Med.* 2016;57:46-53.

19. Vallabhajosula S, Nikolopoulou A, Jhanwar YS, et al. Radioimmunotherapy of metastatic prostate cancer with (1)(7)(7)Lu-DOTAhuJ591 anti prostate specific membrane antigen specific monoclonal antibody. *Curr Radiopharm.* 2016;9:44-53.

20. Weineisen M, Schottelius M, Simecek J, et al. 68Ga- and 177Lu-labeled PSMA I&T: Optimization of a PSMA-targeted theranostic concept and first proof-of-concept human studies. *J Nucl Med.* 2015;56:1169-1176.

21. Kratochwil C, Giesel FL, Stefanova M, et al. PSMA-targeted radionuclide therapy of metastatic castration-resistant prostate cancer with Lu-177 labeled PSMA-617. *J Nucl Med.* 2016.

22. Mease RC, Foss CA, Pomper MG. PET imaging in prostate cancer: focus on prostate-specific membrane antigen. *Curr Top Med Chem.* 2013;13:951-962.

23. Baccala A, Sercia L, Li J, Heston W, Zhou M. Expression of prostate-specific membrane antigen in tumor-associated neovasculature of renal neoplasms. *Urology.* 2007;70:385-390.

24. Haffner MC, Kronberger IE, Ross JS, et al. Prostate-specific membrane antigen expression in the neovasculature of gastric and colorectal cancers. *Hum Pathol.* 2009;40:1754-1761.

25. Pandit-Taskar N, O'Donoghue JA, Divgi CR, et al. Indium 111-labeled J591 anti-PSMA antibody for vascular targeted imaging in progressive solid tumors. *EJNMMI Res.* 2015;5:28.

26. Nomura N, Pastorino S, Jiang P, et al. Prostate specific membrane antigen (PSMA) expression in primary gliomas and breast cancer brain metastases. *Cancer Cell Int.* 2014;14:26.

27. Denmeade SR, Mhaka AM, Rosen DM, et al. Engineering a prostate-specific membrane antigen-activated tumor endothelial cell prodrug for cancer therapy. *Sci Transl Med.* 2012;4:140ra186.

28. DiPippo VA, Olson WC, Nguyen HM, Brown LG, Vessella RL, Corey E. Efficacy studies of an antibody-drug conjugate PSMA-ADC in patient-derived prostate cancer xenografts. *Prostate.* 2015;75:303-313.

29. Slovin SF, Kehoe M, Durso R, et al. A phase I dose escalation trial of vaccine replicon particles (VRP) expressing prostate-specific membrane antigen (PSMA) in subjects with prostate cancer. *Vaccine.* 2013;31:943-949.

30. Cho SY, Gage KL, Mease RC, et al. Biodistribution, tumor detection, and radiation dosimetry of 18F-DCFBC, a low-molecular-weight inhibitor of prostate-specific membrane antigen, in patients with metastatic prostate cancer. *J Nucl Med.* 2012;53:1883-1891.

31. Eiber M, Maurer T, Souvatzoglou M, et al. Evaluation of hybrid 68Ga-PSMA ligand PET/CT in 248 patients with biochemical recurrence after radical prostatectomy. *J Nucl Med.* 2015;56:668-674.

32. Zechmann CM, Afshar-Oromieh A, Armor T, et al. Radiation dosimetry and first therapy results with a (124)I/ (131)I-labeled small molecule (MIP-1095) targeting PSMA for prostate cancer therapy. *Eur J Nucl Med Mol Imaging.* 2014;41:1280-1292.

33. Tagawa ST, Milowsky MI, Morris M, et al. Phase II study of Lutetium-177-labeled anti-prostate-specific membrane antigen monoclonal antibody J591 for metastatic castration-resistant prostate cancer. *Clin Cancer Res.* 2013;19:5182-5191.

34. Afshar-Oromieh A, Babich JW, Kratochwil C, et al. The rise of PSMA ligands for diagnosis and therapy of prostate cancer. *J Nucl Med.* 2016;57:79S-89S.

35. Milowsky MI, Nanus DM, Kostakoglu L, et al. Vascular targeted therapy with anti-prostate-specific membrane antigen monoclonal antibody J591 in advanced solid tumors. *J Clin Oncol.* 2007;25:540-547.

36. Kinoshita Y, Kuratsukuri K, Landas S, et al. Expression of prostate-specific membrane antigen in normal and malignant human tissues. *World J Surg.* 2006;30:628-636.

37. Chen Y, Chatterjee S, Lisok A, et al. A PSMA-targeted theranostic agent for photodynamic therapy. *J Photochem Photobiol B.* 2017;167:111-116.

38. Demirci E, Ocak M, Kabasakal L, et al. (68)Ga-PSMA PET/CT imaging of metastatic clear cell renal cell carcinoma. *Eur J Nucl Med Mol Imaging.* 2014;41:1461-1462.

39. Morris MJ, Divgi CR, Pandit-Taskar N, et al. Pilot trial of unlabeled and indium-111-labeled anti-prostate-specific membrane antigen antibody J591 for castrate metastatic prostate cancer. *Clin Cancer Res.* 2005;11:7454-7461.

FIGURE LEGENDS

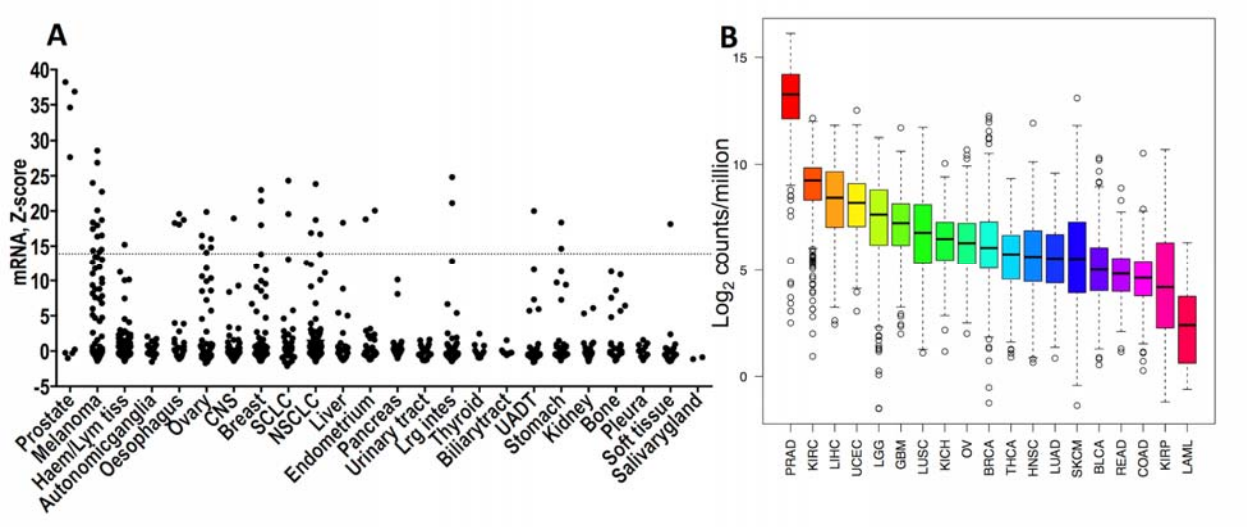

Figure 1. PSMA expression in human tumors. **A**, *FOLH1* gene expression in the cell lines extracted from the CCLE database, converted into z-score, and plotted based on cancer type. Dot plot with a line at median value of prostate cancer cell lines is shown. **B**, Expression of *FOLH1* in different tissue types from TCGA RNAseqV2 data. The dots on the top and bottom of the box represent outliers. The bar at the top and bottom of each box, represents the minimum and maximum expression values of *FOLH1* gene excluding outliers. The box represents 50% of the samples. The horizontal bold line inside the box is the median value of t*FOLH1* expression in the disease type. PRAD – prostate adenocarcinoma; KIRC – kidney renal clear cell carcinoma; LIHC – liver hepatocellular carcinoma; UCEC – uterine corpus endometrial carcinoma; LGG – brain lower grade glioma; GBM – glioblastoma multiforme; LUSC – lung squamous cell carcinoma; KICH – kidney chromophobe; OV, ovarian carcinoma; BRCA – breast invasive carcinoma; THCA – thyroid carcinoma; HNSC – head and neck squamous cell carcinoma; LUAD – lung adenocarcinoma; SKCM – skin cutaneous melanoma; BLCA – bladder urothelial carcinoma; READ – rectum adenocarcinoma; COAD – colon adenocarcinoma; KIRP – kidney renal papillary cell carcinoma; LAML – acute myeloid leukemia.

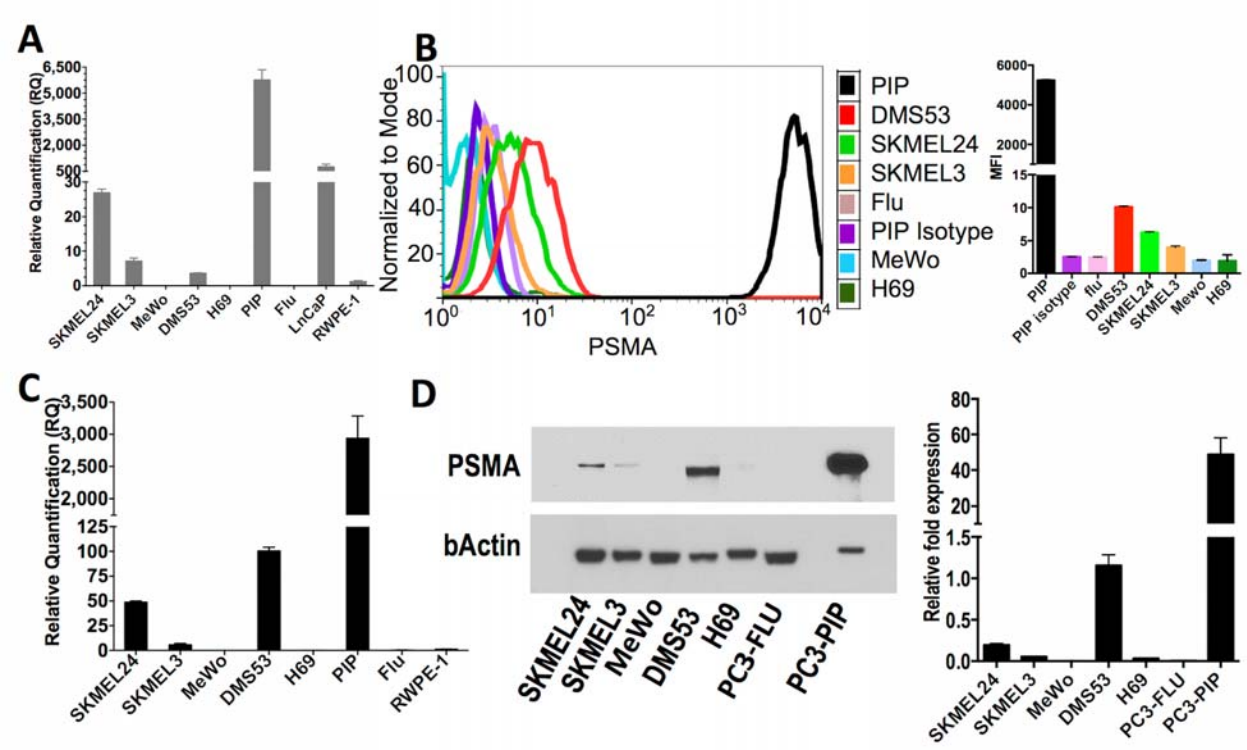

Figure 2. Validation of PSMA expression in non-prostatic human cancer cell lines and xenografts. **A**, PSMA gene expression in selected melanoma and lung cancer cell lines. **B**, Flow cytometry of PSMA surface expression in PSMA+ PC3 PIP, PSMA- PC3 flu and in non-prostatic cancer cell lines. PSMA+ PC3 PIP is designed to overexpress copious amounts of PSMA. The mean fluorescence intensity (MFI) quantification shows that PSMA+ PC3-PIP has a high level of PSMA surface expression whereas PSMA- PC3-flu, MeWo, and H69 are negative and DMS53, SKMEL24, and SKMEL3 are positive (right panel). **C**, PSMA gene expression in selected melanoma and lung cancer xenografts. **D**, PSMA total protein levels in selected melanoma and lung cancer xenografts and the densitometric quantification (**right panel**).

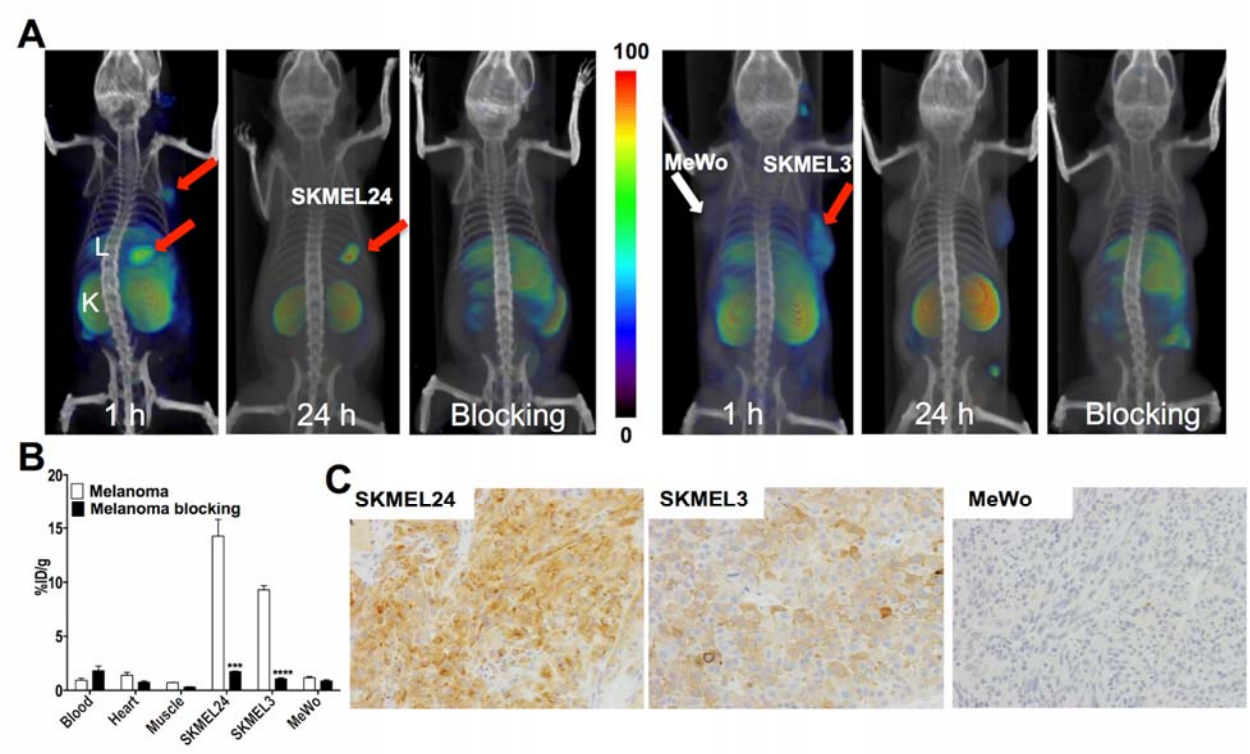

Figure 3. PSMA imaging in subcutaneous melanoma xenografts with the known PSMA-specific radiotracer, ^{125}I-DCIBzl. A, Male NOD/SCID mice bearing SKMEL24 xenografts or SKMEL3 and MeWo were injected with 37 MBq (1 mCi) of ^{125}I-DCIBzl through the tail vein and SPECT/CT images were acquired one and 24 h later. Arrows, tumor; L, liver; K, kidney. **B**, Mice harboring SKMEL24 or SKMEL3 and MeWo xenografts were administered 74 kBq (20 µCi) of ^{125}I-DCIBzl *via* tail vein injection and biodistribution studies were performed at one hour post-injection. For the blocking dose, DCIBzL at 50 mg/Kg was injected s.c. 30 min prior to ^{125}I-DCIBzl. Data are means ± SEM. The significance of the value is indicated by asterisks (*) and the comparative reference is the blocking dose uptake in the same tumor. ***P < 0.001, ****P < 0.0001. **C**, Representative microscopic images of PSMA-stained sections from same cohort of mice obtained at 20X magnification.

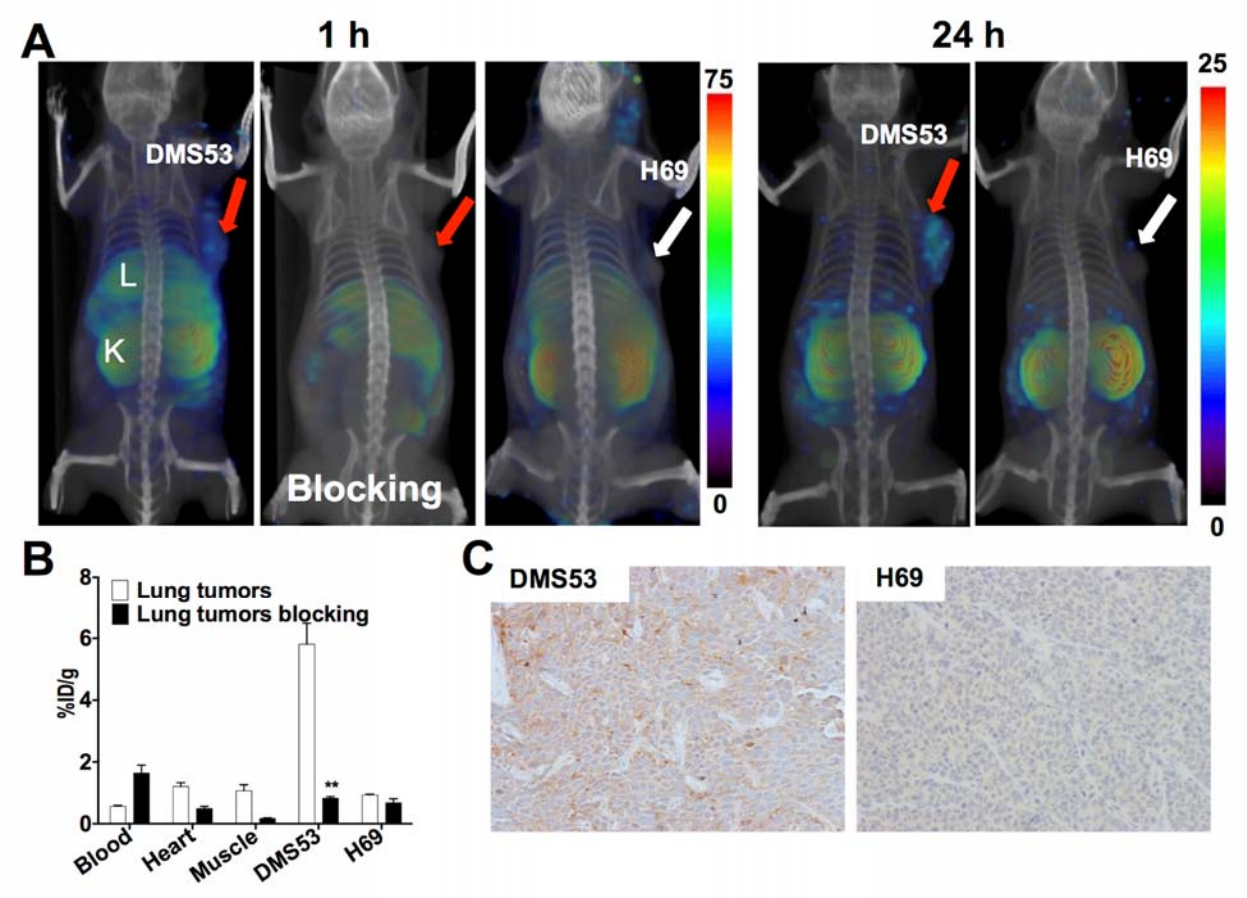

Figure 4. PSMA imaging in subcutaneous lung cancer xenografts with the known PSMA-specific radiotracer, ^{125}I-DCIBzl. A, Male NOD/SCID mice bearing DMS53 or H69 xenografts were administered 37 MBq (1 mCi) of ^{125}I-DCIBzl *via* tail vein injection and SPECT/CT images were acquired at 1 h and 24 h (**right panels**) post injection of the tracer. Arrows, tumor; L, liver; K, kidney. **B**, Mice harboring DMS53 or H69 xenografts were administered 74 kBq (20 µCi) of ^{125}I-DCIBzL and biodistribution was performed at one hour post-injection. For the blocking dose, DCIBzL at 50 mg/Kg was co-injected with ^{125}I-DCIBzl. Data are means ± SEM of four animals. The significance of the value is indicated by asterisks (*) and the comparative reference is the blocking dose uptake in the same tumor $^{**}P < 0.01$. **C**, Representative microscopy images of PSMA-stained sections from same cohort of mice obtained at 20X magnification.

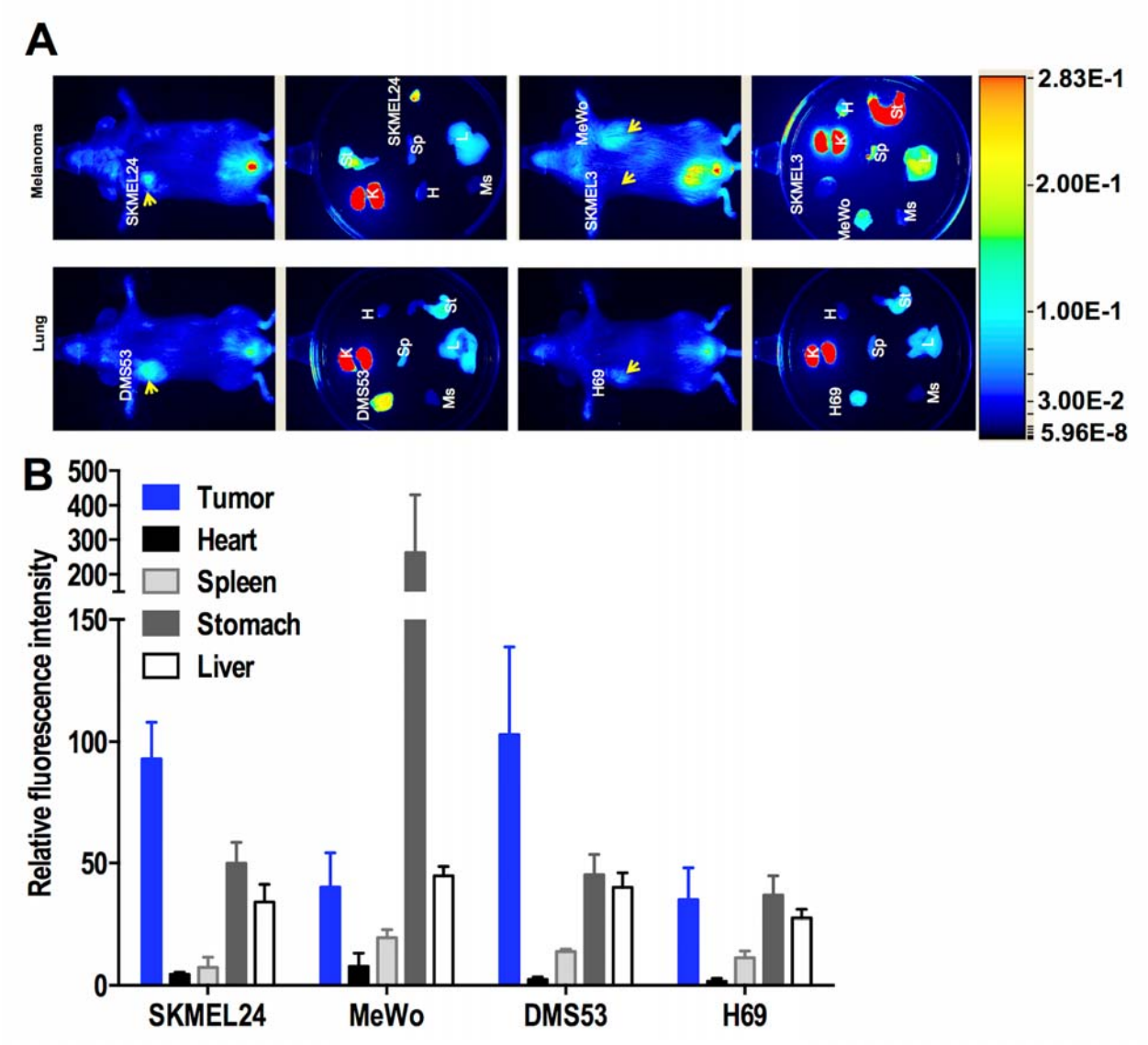

Figure 5. NIR fluorescence imaging of PSMA expression in subcutaneous melanoma and lung xenografts with YC-27. A, Male NOD/SCID mice bearing melanoma and lung xenografts were administered one nanomole of the NIR-labeled PSMA-targeting reagent, YC-27, *via* tail vein injection and fluorescence images were acquired at 24 h post-injection of the imaging agent. **B**, Following NIR imaging, selected tissues were harvested and fluorescence intensity was measured and normalized to the muscle fluorescence intensity. Arrow, tumor; H, heart; K, kidney; L, liver; Ms, muscle; Sp, spleen; St, stomach.

Supplemental Data

SPECT-CT imaging. An X-SPECT small animal single photon emission computed tomography/computed tomography (SPECT/CT) system (Gamma Medica, Northridge, CA) was used for image acquisition. For each tumor model, three mice were used for imaging studies. After an intravenous injection of 37 MBq (1 mCi) of [^{125}I]DCIBzl , images were acquired at 1 h and 24 h post-injection. The SPECT projection data were acquired using two low energy, high resolution parallel-hole collimators with a radius-of-rotation of 6.5 cm. Tomographic data were acquired in 64 projections over 360 degrees at 40 sec/projection. Following tomography, CT imaging was acquired in 512 projections to allow anatomic co-registration. Data were reconstructed using the ordered subsets-expectation maximization algorithm and volume rendered images were generated using Amira 5.3.0 software (Visage Imaging Inc). For blocking studies, 50 mg/kg of non-radiolabeled DCIBzl was co-injected with radiolabeled [^{125}I]DCIBzl.

Fluorescence imaging. Tumor-bearing mice were injected with 1 nmol of **YC-27** and optical images were acquired on the LI-COR Pearl Impulse Near-IR Imager at 24 h post-injection. Following image acquisition, animals were sacrificed and their organs (tumors, muscle, liver, spleen, kidneys, stomach and heart) were assembled on a petri dish and *ex vivo* images were acquired. At least four mice were imaged per tumor model. For image quantification, regions of interest (ROI) were drawn over all organs *ex vivo* and signal intensity was calculated using the manufacturer's software. Uptake in individual organs was normalized to the muscle uptake.

***Ex vivo* biodistribution**. Tumor-bearing mice were injected intravenously with 0.74 mCi (27.4 MBq) of [^{125}I]DCIBzl. At 1 h post-injection mice were sacrificed by cervical dislocation and tumors, blood, heart, lungs, liver, spleen, kidneys and muscle were collected, weighed and counted in a gamma counter. The percentage of injected dose per gram (%ID/g) was calculated based on a standard dose of the injection that was administered to each mouse. At least four mice were used per tumor model.

Quantitative reverse transcription PCR (RT-qPCR)

For mRNA extraction, cell lines were cultured to 80% confluence in 10 cm cell culture dishes and lysed using buffer RLT (Qiagen) containing 1:1000 β-mercaptoethanol (BME). mRNA was extracted from the cell lysate using RNeasy mini kit (Qiagen) and eluted into 40 µL RNAse-free water. For mRNA extraction, tumors were suspended in buffer RLT containing BME and lysed using a micro-homogenizer on ice. After homogenization, samples were centrifuged and the supernatant was employed for mRNA extraction as described above. Following isolation, samples were quantified for mRNA using the Nanodrop™ (Thermo Scientific). About 2.5 µg of each mRNA sample was used to prepare cDNA using the High Capacity cDNA Reverse Transcriptase Kit (Life Technologies) in a total volume of 50 µL as per the manufacturer's recommended protocol. The resultant cDNA samples were used to determine the gene expression by RT-qPCR (FOLH1 Taqman probe, Life Technologies) with GAPDH as an internal control. Relative gene expression was calculated using the ddct method. *FOLH1* expression in cell lines was normalized to the gene expression of the RWPE-1 cells and that in tumors to the PSMA- PC3 flu tumors.

Western blot

Tumor samples were homogenized on ice using RIPA buffer (Sigma Aldrich) containing protease inhibitor cocktail and subsequently sonicated to obtain a clear lysate. After centrifugation to remove cell debris, samples were quantified using the BCA protein assay kit (Thermo Fisher Scientific). About 20 µg of each sample was separated on a 10% Bis-Tris gel (Life Technologies) and transferred onto a nitrocellulose membrane. The membrane blot was blocked in tris-buffered saline containing 5% milk and 0.05% Tween-20 for 1 h at room temperature. PSMA protein expression was visualized using anti-PSMA antibody (Cat # 12702S, Cell Signaling) at a concentration of 1:1000 and β-actin was used as a loading control. For the PSMA+ PC3 PIP tumor sample, only 2.5 µg of total tumor protein was separated on the gel.

Immunohistochemistry

All tumors were harvested from mice and fixed in 10% buffered formalin after which they were embedded in paraffin and sectioned at 5 µm thickness. Tumor sections were de-paraffinized using gradient alcohols and hydrated. Antigen retrieval to unmask the epitopes was performed by steaming the slides in 10 mM citrate buffer (pH 6.0) for 20 min after which they were treated with 3% H_2O_2 solution (DAKO) for 10 min. Slides were blocked with 10% fetal bovine serum in PBS solution for 30 min followed by overnight incubation with prediluted primary anti-hPSMA antibody (Cat# N1611, Dako). The slides were washed and then incubated with secondary universal antibody from the DAKO LSAB+ kit (Cat # K0679) for 1 h. Subsequently, 3, 3'-diaminobenzidine staining was developed according to the manufacturer's protocol. Sections were counterstained with Gill's hematoxylin followed by dehydration with alcohols and xylene and mounted with a cover slip.

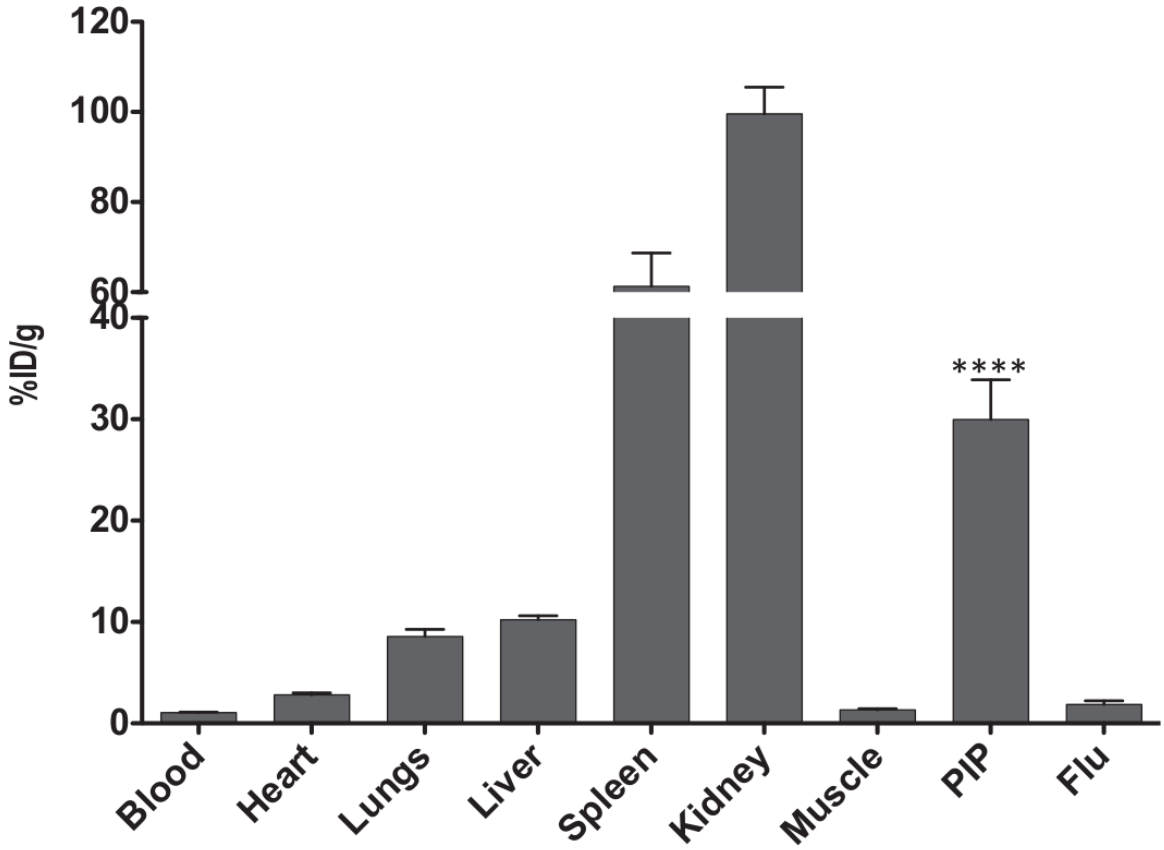

Supplemental Figure 1: **Biodistribution of ^{125}I-DCIBzL in prostate cancer xenografts.** Male NOD/SCID mice harboring PIP and Flu xenografts were administered 74 kBq (20 µCi) of ^{125}I-**DCIBzL** *via* tail vein injection. At one hour post-injection, selected tissues and tumors were harvested, weighed and radioactivity was counted in gamma spectrometer.

All the values were converted into percentage of injected dose per gram of tissue (%ID/g). Data are means ± SEM. The significance of the value is indicated by asterisks (*) and the comparative reference is the blocking dose uptake in the same tumor. ****$P <$ 0.0001.

Tissue	number_patients_>_prostate_min(excluding_outliers)	Total	% of Total excluding PCa	Proportion
PRAD	**457**	**471**		**97.0%**
KIRC	345	604	5.06%	57.1%
LIHC	125	319	1.83%	39.2%
UCEC	50	194	0.73%	25.8%
LGG	98	468	1.44%	20.9%
LUSC	64	541	0.94%	11.8%
SKCM	30	333	0.44%	9.0%
GBM	14	174	0.21%	8.0%
OV	14	266	0.21%	5.3%
KIRP	11	273	0.16%	4.0%
KICH	3	91	0.04%	3.3%
BRCA	38	1172	0.56%	3.2%
HNSC	16	540	0.23%	3.0%
BLCA	5	329	0.07%	1.5%
COAD	1	314	0.01%	0.3%
LUAD	1	452	0.01%	0.2%
THCA	1	565	0.01%	0.2%
READ	0	101	0.00%	0.0%
LAML	0	82	0.00%	0.0%
TOTAL	**816**	**6818**	**12.0%**	